Characterizing Complex Dynamics in the Transactivation Response Element Apical Loop and Motional Correlations with the Bulge by NMR, Molecular Dynamics, and Mutagenesis

Elizabeth A. Dethoff,* Alexandar L. Hansen,* Catherine Musselman,* Eric D. Watt,* Ioan Andricioaei,† and Hashim M. Al-Hashimi*

*Department of Chemistry and Biophysics, University of Michigan, Ann Arbor, Michigan 48109-1055; and †Department of Chemistry, University of California, Irvine, California 92697

ABSTRACT The HIV-1 transactivation response element (TAR) RNA binds a variety of proteins and is a target for developing anti-HIV therapies. TAR has two primary binding sites: a UCU bulge and a CUGGGA apical loop. We used NMR residual dipolar couplings, carbon spin relaxation (R_1 and R_2), and relaxation dispersion ($R_{1\rho}$) in conjunction with molecular dynamics and mutagenesis to characterize the dynamics of the TAR apical loop and investigate previously proposed long-range interactions with the distant bulge. Replacement of the wild-type apical loop with a UUCG loop did not significantly affect the structural dynamics at the bulge, indicating that the apical loop and the bulge act largely as independent dynamical recognition centers. The apical loop undergoes complex dynamics at multiple timescales that are likely important for adaptive recognition: U31 and G33 undergo limited motions, G32 is highly flexible at picosecond-nanosecond timescales, and G34 and C30 form a dynamic Watson-Crick basepair in which G34 and A35 undergo a slow (~30 μs) likely concerted looping in and out motion, with A35 also undergoing large amplitude motions at picosecond-nanosecond timescales. Our study highlights the power of combining NMR, molecular dynamics, and mutagenesis in characterizing RNA dynamics.

INTRODUCTION

The transactivation response element (TAR) RNA hairpin (1) (Fig. 1 *a*) plays a diverse role in HIV viral replication and is a major target for developing anti-HIV therapies (2). TAR has two primary binding sites: a trinucleotide bulge and hexanucleotide apical loop. The bulge binds the viral transactivator protein Tat (3), which stimulates transcription elongation of HIV messenger RNA by recruiting the positive transcription elongation factor (4,5). The TAR apical loop contacts the positive transcription elongation factor via the cyclin T1 subunit (4–7) and is also believed to bind a number of other proteins, including the TAR RNA-binding protein, which inhibits protein kinase R (8,9) and increases RNA translation (2,10), the nucleocapsid protein, which promotes minus-strand transfer during reverse transcription (11), and the eukaryotic translation initiation factor 2, which is believed to contact both the TAR apical loop and the subapical lower stem (12). The apical loop is also believed to aid dimerization of the HIV-1 genome by forming self-interactions in kissing complexes (13,14).

Most biophysical studies have so far focused on characterizing the conformational properties of the TAR bulge where the protein Tat binds. Studies have shown that recognition of TAR by Tat-derived peptides results in large changes in the relative orientation of helices that are coupled to local rearrangements in the bulge conformation (15–19). Numerous studies have also established that the TAR bulge can adopt wide-ranging conformations and thereby bind to a variety of targets including divalent ions (20,21) and chemically distinct small molecules that bind the HIV-1 TAR bulge and inhibit its interaction with Tat (22–25). Recent studies show that inherent flexibility at the bulge junction plays an important role in adaptive recognition (26–32). In particular, new domain elongation NMR techniques allowed resolution of interhelical motions and local fluctuations in and around the bulge that mirror the structural rearrangements that take place upon recognition (28,29). Thus, small molecules likely select conformers in the TAR dynamical ensemble by ''tertiary capture'' rather than inducing new TAR conformations (28,29). These NMR studies were focused on the TAR bulge and were conducted on a TAR mutant (TAR_m) in which the wild-type (wt) apical loop was replaced with a spectroscopically more favorable UUCG tetraloop (33) (Fig. 1 *a*).

Few biophysical studies have examined the TAR apical loop which is also being targeted in the design of anti-HIV therapeutics (34–37). No structures have been reported to date for the TAR apical loop when in complex with cognate protein targets. Available structures of TAR show significant differences in the apical loop conformation likely because it is highly flexible in solution. To date, no quantitative experiments have been performed to characterize dynamics in the apical loop and its potential roles in adaptive recognition. Furthermore, studies provide evidence for long-range inter-

Submitted June 16, 2008, and accepted for publication June 19, 2008.

Address reprint requests to Hashim M. Al-Hashimi, Tel.: 734-615-3361; Fax: 734-647-4865; E-mail: hashimi@umich.edu.

Catherine Musselman's present address is Dept. of Pharmacology, University of Colorado Health Sciences Center, Aurora, CO 80045.

Eric D. Watt's present address is Dept. of Chemistry, Yale University, 225 Prospect Street, New Haven, CT 06520-8107.

Editor: Samuel Butcher.

0006-3495/08/10/3906/10 $2.00

doi: 10.1529/biophysj.108.140285

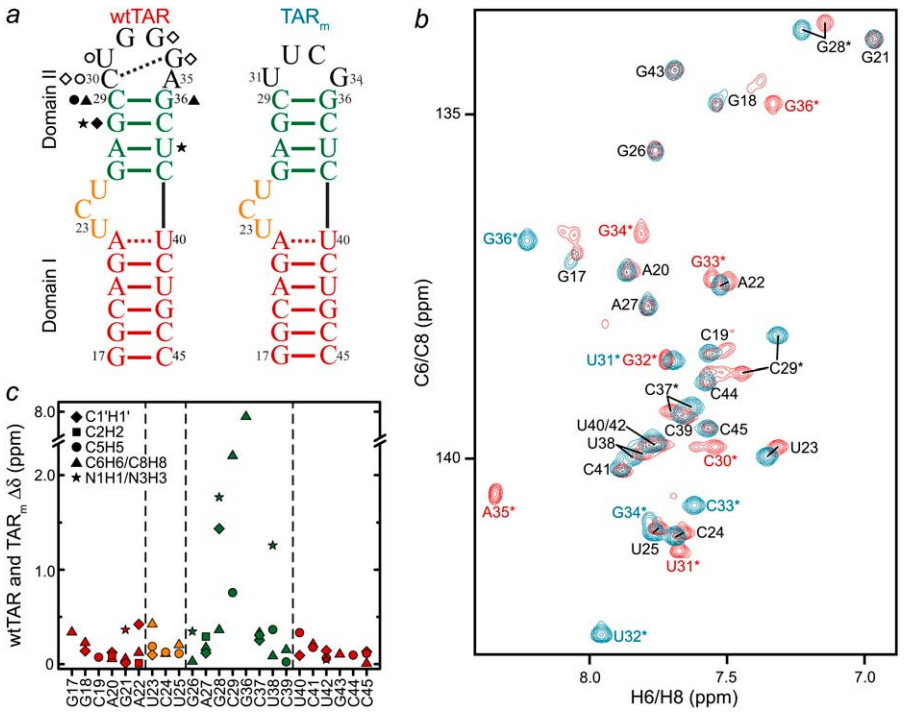

FIGURE 1 NMR chemical shift comparison of wtTAR and TAR$_m$. (*a*) Secondary structures of wtTAR and TAR$_m$. Residues with the largest chemical shift perturbations (>0.25 ppm) between wtTAR and TAR$_m$ are highlighted on the wtTAR secondary structure using solid black symbols. Apical loop residues that undergo significant chemical shift perturbations upon ARG binding are highlighted in open black symbols. See inset in *c* for symbol key. (*b*) 2D ^{1}H-^{13}C HSQC spectra of wtTAR (*red*) overlaid on corresponding spectra of TAR$_m$ (*blue*). Asterisks and colored labels denote resonances that are different between wtTAR and TAR$_m$ due to the loop mutation. (*c*) Chemical shift differences ($\Delta\delta = \sqrt{(\Delta\delta_H)^2 + (\alpha\Delta\delta_X)^2}$, where $\Delta\delta_H$ and $\Delta\delta_X$ are the changes in proton and carbon/nitrogen chemical shift and α is the ratio of the H and C/N gyromagnetic ratio) between wtTAR and TAR$_m$.

actions between the apical loop and the bulge (38,39) that could make the conformational dynamics of wt TAR (wtTAR) different from that of TAR$_m$, which has previously been studied by NMR. Based on sequence covariation, structure probing, and molecular modeling, Berkhout and co-workers proposed that apical loop residue U31 forms a U31·A22-U40 base-triple in unbound TAR involving the A22-U40 basepair in domain I (38). Isotropic reorientational eigenmode dynamics analysis of a 20 ns molecular dynamics (MD) simulation of wtTAR revealed that dynamics at the apical loop, particularly residue U31, is correlated by unknown mechanisms to dynamics at the bulge, particularly residues U23 and C24 (39). Such long-range interactions may provide the basis for coupling recognition events at the different TAR binding sites and may account in part for the high cooperativity of Tat and cyclin T1 binding to these two different TAR sites (7). Long-range motional correlations are increasingly implicated in the functions of RNA (40,41) but are notoriously difficult to characterize based on experimental methods.

Here, we report the NMR and MD characterization of the conformational dynamics of the wtTAR apical loop and use a mutagenesis approach to experimentally examine potential couplings it may have to the trinucleotide bulge. Our results show that the apical loop and bulge act as independent dynamical centers with the apical loop undergoing complex dynamics at multiple timescales that are likely important for adaptive recognition. Our study establishes an NMR experimental framework for studying motional correlations in RNA and indentifies one approach for indirectly establishing motional correlations between distinct regions in RNA.

MATERIALS AND METHODS

Preparation and purification of uniformly ^{13}C/^{15}N-labeled RNA

E-AU-wtTAR, E-GC-wtTAR, and wtTAR samples were prepared by in vitro transcription using T7 RNA polymerase (Takara Mirus Bio, Madison, WI), uniformly ^{13}C/^{15}N-labeled nucleotide triphosphates (ISOTEC, Miamisburg, OH), unlabeled nucleotide triphosphates (Sigma, St. Louis, MO), and synthetic DNA templates (Integrated DNA Technologies, Coralville, IA) containing the T7 promoter and sequence of interest. Short and elongated RNAs were purified using 20% and 15% (w/v) denaturing polyacrylamide gel electrophoresis, respectively, with 8 M urea and Tris-Borate-EDTA buffer. The RNA was eluted from the gel in 20 mM Tris pH 8 buffer followed by ethanol precipitation. The RNA pellet was dissolved in water and exchanged into NMR buffer (15 mM sodium phosphate, 0.1 mM EDTA, and 25 mM NaCl at pH ~6.4) multiple times using a Centricon Ultracel YM-3 concentrator (Millipore, Bedford, MA). The elongated samples were annealed at 95°C for 5 min before being exchanged into NMR buffer. The final RNA concentration of the E-AU-wtTAR, E-GC-wtTAR, and wtTAR samples was 1.5 mM, 0.5 mM, and 0.7 mM, respectively. The aligned NMR sample of wtTAR was prepared by adding Pf1-phage (Asla Biotech, Riga, Latvia) in NMR buffer to wtTAR to yield a final Pf1-phage concentration of ~19 mg/mL and a final RNA concentration of 0.35 mM. The addition of phage did not affect the average structure of RNA as judged from careful comparison of the chemical shifts in the absence and presence of phage (data not shown).

Resonance assignments

All NMR experiments were performed at 298 K on an Avance Bruker (Billerica, MA) 600 MHz spectrometer equipped with a triple-resonance cryogenic (5 mm) probe and an Avance Bruker 900 MHz spectrometer equipped with a TCI cryoprobe. NMR spectra were analyzed using NMRPipe/NMRDraw (42) and Sparky 3 (43). The ^{1}H-, ^{13}C-, and ^{15}N-resonances in wtTAR were assigned using standard homonuclear and heteronuclear, two-dimensional (2D) and three-dimensional (3D) experiments (44) on unlabeled and uniformly ^{13}C/^{15}N-labeled wtTAR sample, respectively. The non-

exchangeable nuclear Overhauser effect (NOE) walk was uninterrupted from C19 to U23, G26 to C29, and G34 to C39, indicating a continuous helical conformation in these regions. The NOE walk was interrupted at bulge residue C24 and apical loop residue C30 and became convoluted at the terminal ends due to peak multiplicity and end-fraying effects. The nuclear Overhauser effect spectroscopy data were supplemented with 3D HCN experiments (45) for intranucleotide H8/H6-N1/N9 H1′ correlations and a 2D HCCNH experiment (46) for base C6/C5 to imino H1/H3 correlations in pyrimidines. All resonance intensities in E-wtTAR were measured as previously described for E-TAR$_m$ (29). Values for various bond vector types were normalized to a minimum value of 0.1 independently for G-C and A-U residues, as previously described (29).

Measurement and order tensor analysis of RDCs

2D ^{13}C-^{1}H (or ^{15}N-^{1}H) S^{3}E heteronuclear single quantum coherence (HSQC) experiments (47,48) were used to measure one-bond $^{1}D_{C6H6}$, $^{1}D_{C8H8}$, $^{1}D_{C5H5}$, $^{1}D_{C2H2}$, $^{1}D_{C1'H1'}$, and $^{1}D_{N1/3H1/3}$ residual dipolar couplings (RDCs) in nonelongated wtTAR using ~19 mg/ml of Pf1-phage (49,50) as an ordering medium. RDC measurement error was estimated from duplicate experiments that yielded splittings along the ^{1}H dimension or ^{15}N/^{13}C dimension, as previously described (51,52). The measured RDCs are listed in Table S1 in Supplementary Material, Data S1.

The RDCs measured in Watson-Crick basepairs in domains I and II were subjected to an order tensor analysis using idealized A-form helices as input coordinates (53). Statistics for this analysis are summarized in Table 1. RDCs from the flexible residues G17-C45, and A22-U40 were excluded from analysis (53). The helices were constructed using the Biopolymers module in Insight II (Molecular Simulations, San Diego, CA), followed by a correction of the propeller twist angles from +15° to the idealized A-form value of −15° (53,54). The measured RDCs and idealized A-form helices were used to determine best-fit order tensors for each domain using singular value decomposition (55) implemented by the in-house written program RAMAH (56). Order tensor errors due to ''A-form structural noise'' and RDC uncertainty were estimated using the program AFORM-RDC (53). The overall RNA structure was assembled by rotating each domain into the principal axis system of the best-fitted order tensor. The helices were then assembled using the program Insight II (Molecular Simulations). Three of the four possible interhelical orientations were omitted because they resulted in U40 (P)-C39 (O3′) and A22 (O3′)-G26 (P) distances >1.59 Å and >28 Å, respectively. Interhelical angles for all RNA structures were calculated using the in-house program Euler-RNA as previously described (57).

Measurement of nucleobase carbon relaxation

The power dependence of $R_{1\rho}$ was measured for nucleobase C2, C6, and C8 carbons at 25°C using the pulse sequence shown in Fig. S1 in Data S1. The same pulse sequence was used to measure R_1 by replacing the ^{13}C spinlock and adiabatic passages with a series of high power ^{1}H 180° pulses separated by 10 ms. A total of 10 and 6 relaxation decays were measured for wtTAR and TAR$_m$, respectively, with spinlock strengths ranging from 1 to 5 kHz and at three different offsets (Table S2 in Data S1). The power dependence of the observed $R_{1\rho}$ was fitted using

$$R_{1\rho} = R_1\cos^2(\theta) + R_2^0\sin^2(\theta) + \frac{\sin^2(\theta)\varphi_{ex}k_{ex}}{\omega_{eff}^2 + k_{ex}^2},$$

where $\theta = \arctan(\omega_1/\Omega)$ is the effective tilt angle of the magnetization; ω_1 is the spinlock power; Ω is the chemical shift offset of the resonance from the spinlock frequency; $\omega_{eff} = (\omega_1^2 + \Omega^2)^{1/2}$ is the effective field strength; R_2^0 is the intrinsic transverse relaxation rate; $\phi_{ex} = p_a p_b \Delta\omega^2$, where p_a and p_b are the populations of the exchanging states a and b; $\Delta\omega$ is the difference in chemical shift between the states (rad/s); and k_{ex} is the timescale of the motion (58). To ascertain the presence of exchange in the dispersion curves, F-test statistics were used at the 99% confidence level between one (R_2) and three (R_2, ϕ_{ex}, k_{ex}) parameter fits to the data. For all but the A35 C8 (p-value 3.86×10^{-4}) and G34 C8 (p-value 3.24×10^{-5}) resonances in wtTAR, which share a chemical exchange time of 33.4 ± 5.8 μs, no measurable exchange is observed on the microsecond timescale (see Fig. 4 c and Table S2 in Data S1).

Using the R_2 values measured at the highest power and off-resonance spinlocks, the value of $2R_2 - R_1$ was computed providing an estimate for the amplitudes of picosecond-nanosecond motions. $2R_2 - R_1$ is, to a good approximation, proportional to $S^2 \times J(0)$, where S^2 is the order parameter describing motions occurring faster than overall tumbling of the nucleic acid and $J(0)$ is the spectral density function at zero field. The value of $2R_2 - R_1$ is therefore independent of the timescale of internal motions as well as the number of contributing relaxation mechanisms under the assumption that all relaxation mechanisms experience similar amplitude isotropic motions (59,60). Relative S^2 (S^2_{rel}) values can therefore be estimated from the ratio of $2R_2 - R_1$ measured for each residue to that of the largest value obtained in the well-structured A-form helices (see Fig. 3 e). Orientational dependencies of the ^{13}C relaxation rates for RNA the size of wtTAR are expected to vary $2R_2 - R_1$ by only ~10% (60).

Molecular dynamics simulations

A 65 ns all-atom MD simulation of wtTAR was performed using the CHARMM force field (parameter set 27) (61). Structure 3 of the family of free TAR NMR structures (Protein Data Bank 1ANR) (32) was used as the starting coordinates, chosen as it yields the best agreement with previous RDCs measurements (30). TAR was neutralized using Na^+ counterions and solvated in a 35 Å sphere of TIP3P water site (62). A stochastic boundary potential was used (63), allowing a more than 9 Å distance between the surface of the sphere and all RNA atoms. The solvated system was minimized and heated to 300 K while harmonically constraining the heavy atoms of the RNA with a force constant of 62 kcal/mol/Å^2 for 100 ps, after which the constraints were removed. The system was then preliminarily equilibrated for 1 ns, and a production-run trajectory was followed up to 65 ns. A Nose-Hoover thermostat using a coupling constant of 50 ps^{-1} (64,65) was employed to maintain a constant temperature of 300 K throughout the simulation, with a 1 fs time step. Details of the structural dynamics and correlations from this simulation are reported elsewhere (39,53).

RESULTS AND DISCUSSION

NMR characterization of wtTAR and TAR$_m$

If a long-range conformational coupling exists between the TAR apical loop and bulge, then replacement of the wt CUGGGA apical loop with a UUCG loop should affect the conformational properties of the bulge and therefore its NMR resonances. We first compared 2D HSQC spectra of uniformly ^{13}C/^{15}N-labeled wtTAR with those of the TAR$_m$ (Fig. 1 a). Representative spectra are shown in Fig. 1 b (additional spectra provided in Fig. S3 in Data S1) and the differences in chemical shifts are shown in Fig. 1 c. Expected differences are observed for domain II residues C29, G36, G28, and C37 that are near the apical loop (Fig. 1, b and c). However, significant differences are also observed at the bulge (U23) and neighboring residue A22 in domain I (Fig. 1, b and c). The latter chemical shift differences are very similar in both amplitude and direction to the shifts induced by Na^+ ions and could possibly arise from small differences in sample preparation and from having less Na^+ in wtTAR (52). The difference observed for U38, which is involved in Tat recognition and

TABLE 1 Order tensor analysis of wtTAR RDCs

Domain	*N*	*CN*	RMSD (Hz)	*R*	η	$\vartheta \times 10^{-3}$	ϑ_{int}	θ	ξ
I	14	5.7	1.2	0.99	0.36 ± 0.1	0.65 ± 0.08	0.54 ± 0.07	45 ± 7	−41 ± 50
II	13	3.0	1.7	0.99	0.10 ± 0.05	1.19 ± 0.05			

Order tensor analysis of RDCs measured in the wtTAR helical stems. Shown for each helical stem are the number of RDCs (*N*); condition number (*CN*) (70); root mean-square deviation (RMSD); and correlation coefficient (*R*) between measured and back-predicted RDCs; order tensor asymmetry ($\eta = |S_{yy} - S_{xx}|/S_{zz}$); generalized degree of order ($\vartheta = \sqrt{2/3(S_{xx}^2+S_{yy}^2+S_{zz}^2)}$) (70); internal generalized degree of order (ϑ_{int}) (70); and interhelical bend (θ) and twist (ξ) angles calculated using the program Euler-RNA (57). Errors for η, ϑ, and ϑ_{int} are estimated using the program AFORM-RDC (53).

which is flexible in unbound TAR (29), is likely due to the apical loop mutation. Finally, a greater deal of peak multiplicity is observed for terminal residues G17, G18, and C19 in wtTAR compared TAR_m that most likely arises from the presence of a combination of *n* and *n* + 1 transcripts.

We examined if wtTAR binds the ligand argininamide (ARG), which is used as a mimic of Tat (15,66), in a manner similar to TAR_m. The ARG-induced chemical shift perturbations were virtually identical for wtTAR and TAR_m (Fig. S4 in Data S1), indicating that the apical loop does not affect ARG binding at the bulge. Nevertheless, ARG binding induced small perturbations at the apical loop at a distance from the bulge binding site (Figs. 1 *a* and Fig. S4 in Data S1). The possible source of these perturbations is discussed in a subsequent section.

We did not obtain any evidence for the proposed U31·A22-U40 base triple (38) in unbound wtTAR (Fig. S5 in Data S1). We were unable to observe the U31 imino proton to detect a crosspeak between H5 of U31 and the N7 of A22 using the *trans*-hydrogen bond J_{NN} H5 (C5)NN NMR experiment which employs the nonexchangeable H5 (67) (Fig. S5 in Data S1). Thus, the U31·A22-U40 base triple either does not form or forms only transiently in solution.

Comparison of wtTAR and TAR_m structural dynamics using RDCs

The small differences between spectra of TAR_m and wtTAR raise the possibility that the apical loop influences the bulge conformation and therefore the relative orientation and dynamics of the TAR helices. To this end, we characterized the wtTAR interhelical conformation using one-bond C-H ($^1D_{CH}$) and N-H ($^1D_{NH}$) RDCs (51,68,69) and compared it to the TAR_m conformation reported previously (30). The relative orientation and dynamics of helices was determined using an order tensor analysis (55,57), as reported previously for TAR_m (53). Key statistics for this analysis are summarized in Table 1. Here, order tensors describing partial alignment relative to the magnetic field were determined for each helix by fitting the RDCs measured in nonterminal Watson-Crick basepairs to an idealized A-form helix geometry (53,57). The program AFORM-RDC was used to estimate errors in the order tensor elements arising from ''structural noise'' and RDC measurement uncertainty (53). An excellent fit was observed for the two helices (Fig. 2 *a*), indicating that the two helices adopt a canonical A-form geometry, as previously reported for TAR_m (53).

Superposition of the order tensor frames obtained for each helix allowed determination of their average relative orientation (53,57). As shown in Fig. 2 *b*, the average interhelical bend (θ) and twist (ξ) angles obtained for wtTAR are, within experimental error, identical to those determined for TAR_m (30). The order tensor analysis also yields the amplitude of interhelical motions, as characterized by an internal generalized degree of order ϑ_{int}, which varies between 0 and 1 for maximum and minimum interhelical motional amplitudes, respectively (70). As shown in Fig. 2 *b* and Table 1, $\vartheta_{int} = 0.54 \pm 0.07$ for wtTAR is in excellent agreement with $\vartheta_{int} = 0.56 \pm 0.03$ for TAR_m (30,53). Thus, wtTAR and TAR_m undergo similar amplitude interhelical motions at submilli-

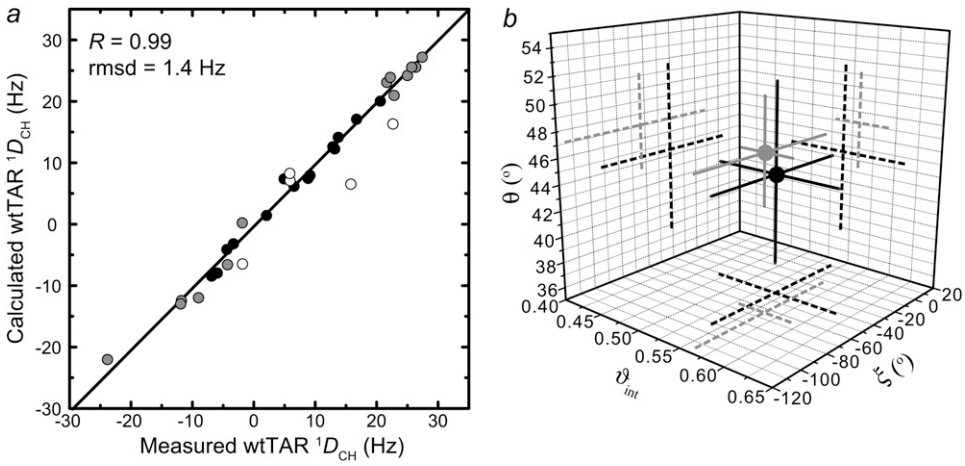

FIGURE 2 RDC-based comparison of the wtTAR and TAR_m conformational dynamics. (*a*) Correlation plot between measured and back-calculated wtTAR RDCs when each stem order tensor is independently fit to an idealized A-form geometry. Domain II is shown in gray, and domain I is shown in black, with A22 and U40 represented by open black circles. (*b*) The values for the interhelical bend (θ), twist angle (ξ), and the interhelical mobility (ϑ_{int}) determined for wtTAR (*black*) and TAR_m (*gray*). Experimental errors are shown.

second timescales. This, together with the similar RDCs observed for the bulge and junctional A22-U40 basepair (data not shown) suggest that TAR_m and wtTAR adopt very similar conformations in solution and therefore that the apical loop does not significantly affect the conformational dynamics of the bulge.

Structural dynamics by ^{15}N and ^{13}C spin relaxation and domain elongation

To further characterize the conformational dynamics of wtTAR at picosecond-nanosecond timescales, we used a domain-elongation strategy to decouple internal motions from overall reorientation (29) (Fig. 3 *a*). The elongation slows down overall rotational diffusion, allowing its separation from internal motions occurring at timescales comparable to overall molecular tumbling of the nonelongated RNA (71). To avoid increasing NMR spectral overlap, two RNA constructs were prepared that are elongated using stretches of either unlabeled A-U (E-AU-wtTAR) or G-C (E-GC-wtTAR) basepairs in a background of uniformly $^{13}C/^{15}N$-labeled G-C or A-U nucleotides, respectively (Fig. 3 *a*).

The E-wtTAR construct more closely resembles TAR in the HIV-1 leader context, where its lower helix is 19 basepairs long. Interestingly, unlike for TAR_m (29), elongation of wtTAR resulted in significant chemical shift changes in residues that are distant from the elongation site, including residues in and around the bulge (A22 and C24) and even the very distant apical loop (C30, U31, G34, and A35) (Fig. 3, *a* and *b*). In contrast, chemical shift perturbations are not observed upon elongation for UUCG loop resonances in TAR_m (72). Compared to the short constructs, spectra of E-wtTAR are in better agreement with those of E-TAR_m, which are in turn very similar to those of TAR_m (29). One possibility is that the wt apical loop transiently interacts with the flexible ter-

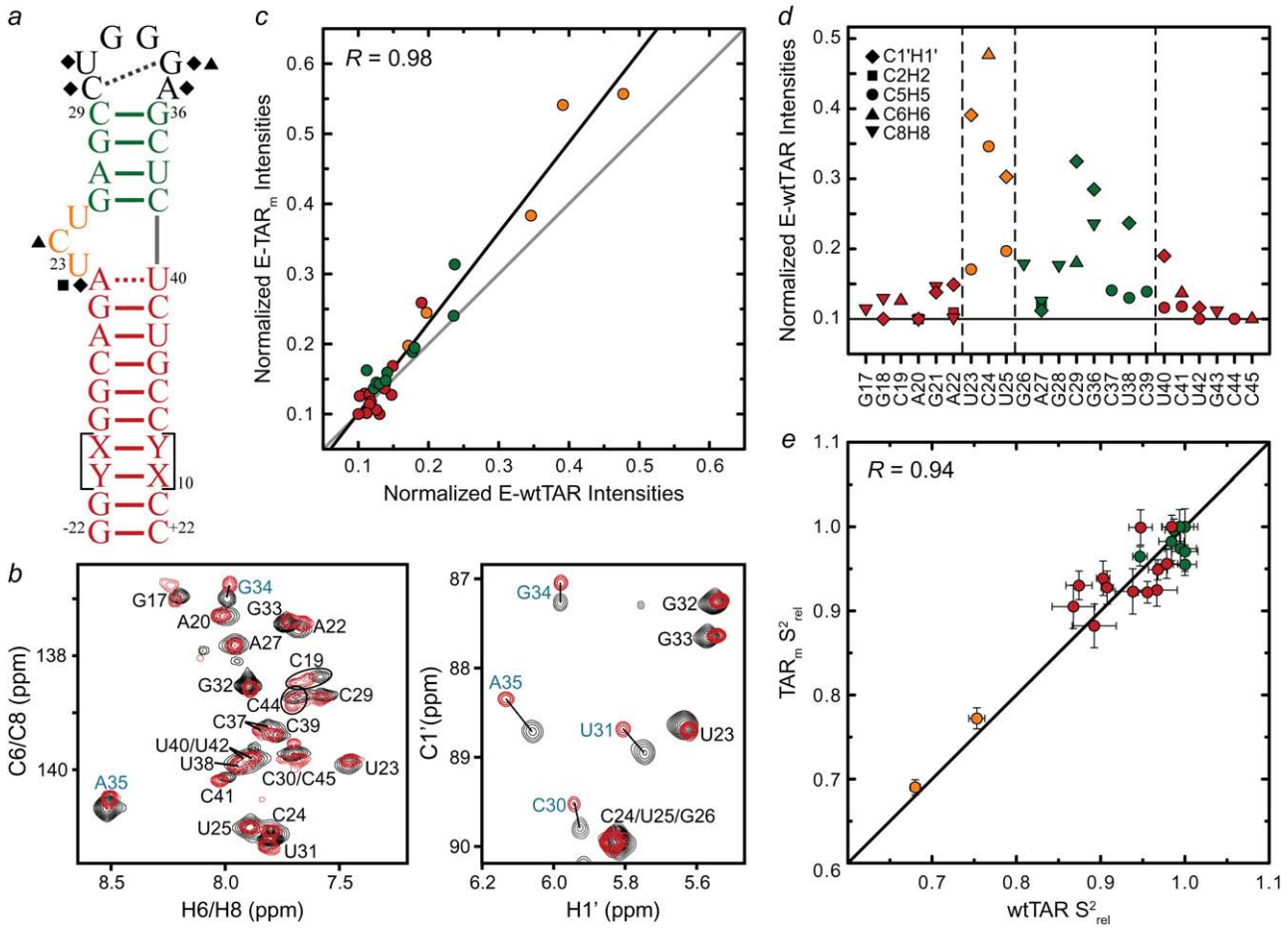

FIGURE 3 Spin relaxation-based comparison of the E-wtTAR and E-TAR_m conformational dynamics. (*a*) Elongated construct of wtTAR in which XY are unlabeled CG (E-GC-wtTAR) and UA (and E-AU-wtTAR) residues as previously described (29). Residues that undergo significant chemical shift perturbations upon elongation are highlighted on the secondary structure using black solid symbols. See inset in Fig. 1 *d* for symbol key. (*b*) 2D HSQC spectra of wtTAR (*red*) overlaid on corresponding spectra of E-AU-wtTAR and E-GC-wtTAR (*black*). Blue labels denote loop resonances that shift upon elongation. (*c*) Correlation plot between the E-wtTAR and E-TAR_m normalized intensities. Shown is the correlation coefficient (*R*). (*d*) Normalized resonance intensities (peak heights) measured from 2D HSQC spectra of E-wtTAR. See inset for key. (*e*) Correlation plot between nucleobase carbon S^2_{rel} values measured in nonelongated wtTAR and TAR_m. Values for domain I, bulge, and domain II are shown in red, orange, and green circles, respectively.

minal basepairs in domain I in short wtTAR and that this interaction is disrupted or altered upon elongation. We observe such a long-range interaction in a 65 ns MD simulation of wtTAR (39), in which apical loop residue A35 for which we see the largest differences in chemical shifts between short and elongated wtTAR (Fig. 3 *b*) come within <3 Å of G17 at the terminal end of the lower helix I (Fig. S6 in Data S1).

The ensemble of NOE NMR structures of unbound wtTAR also include conformations in which the same apical loop residue A35 is in direct contact with the lower region of domain I (32) (Fig. S6 in Data S1). Such a long-range interaction could indirectly influence the bulge conformation and thereby give rise to the motional correlations between the bulge and apical loop dynamics observed in the isotropic reorientational eigenmode dynamics study (39). However, we were unable to detect NOE crosspeaks between the apical loop and terminal resides of domain I in wtTAR. This, and the excellent agreement between the RDC-derived wtTAR and TAR_m conformations (Fig. 2 *b*), indicates that any such long-range interaction does not significantly alter the global dynamics of wtTAR relative to TAR_m. Note that even if present transiently, such a long-range interaction should be considered an artifact of the wtTAR construct design since it is apparently diminished in elongated wtTAR, which more accurately mimics TAR in its native viral context.

We recently reported ^{15}N relaxation measurements on E-wtTAR (C. Musselman, Q. Zhang, H. M. Al-Hashimi, and I. Andricioaei, unpublished). The goal of the latter study was to quantitatively compare the dynamics measured by NMR with those computed by MD. The imino nitrogen spin relaxation order parameters (S^2) describing the amplitude of fast (S_f^2) and slow (S_s^2) picosecond-nanosecond motions obtained for E-wtTAR were very similar to those determined for E-TAR_m (Fig. S7 in Data S1), indicating that the two RNAs have very similar dynamical properties at picosecond-nanosecond timescales. To more fully characterize the dynamics of E-wtTAR, we measured the C-H resonance intensities, which, ignoring chemical exchange, provide a qualitative measure of internal motions occurring at nanosecond and faster timescales (29,60). The normalized E-wtTAR intensities (Fig. 3 *d*) were very similar to those of E-TAR_m (Fig. 3 *c*), again indicating that the two RNAs have very similar dynamical properties. However, the slope of the line deviates from unity (Fig. 3 *c*) and the intensities measured in E-wtTAR, and particularly the bulge and domain II, are consistently lower than those measured in E-TAR_m (Fig. 3 *c*). Though the similar RDCs observed at the bulge and neighboring residues in wt-TAR and TAR_m rule out substantial differences in motional amplitudes at submillisecond timescales, other factors may influence the observed resonances intensities. The bulge and domain II residues in wtTAR may experience a greater deal of chemical exchange broadening. However, based on carbon $R_{1\rho}$ relaxation dispersion experiments, the only significant exchange contribution is observed in the apical loop of wtTAR, with little to no exchange observed in the bulge region in both TAR_m and wtTAR (Fig. S2 in Data S1).

We also measured longitudinal (R_1) and transverse (R_2) spin relaxation rates for the nucleobase carbons C2, C6, and C8 in the short wtTAR and TAR_m. Qualitative relative order parameters (S_{rel}^2) were determined based on the computation of $2R_2 - R_1$ (see Materials and Methods), which is largely independent of motional timescales (59,60). Good agreement is observed between the S_{rel}^2values obtained for TAR_m and wtTAR, which show little to no systematic differences (Fig. 3 *e*). The slope deviation in the resonance intensities observed in the elongated constructs (Fig. 3 *c*) may be due to slower motional timescales for wtTAR, which arise possibly due to its larger and more flexible apical loop. Indeed, analysis of ^{15}N relaxation data indicates that the domain motions are slightly slower in E-wtTAR ($\tau_s = 20.7$ ns) (C. Musselman, Q. Zhang, H. M. Al-Hashimi, and I. Andricioaei, unpublished) compared to E-TAR_m ($\tau_s = 18.9$ ns) (29).

Complex dynamics in the apical loop

Our NMR data revealed complex dynamics over a broad range of timescales in the apical loop. The apical loop RDCs yielded very poor fits to available HIV-1 TAR structures (1ANR, 1ARJ, 1AJU, 1QD3, 1UTS, 1LVJ, 1AKX, 1UUI, and 1UUD (22–25,32,74,75)) likely due to the presence of internal motional averaging contributions (data not shown).

Very high resonance intensities in E-wtTAR (Fig. 4 *a*), low $2R_2 - R_1$ values (Fig. 4 *a*), and near zero RDCs (Fig. 4 *b*) indicative of high internal mobility at the picosecond-nanosecond timescales were observed for both base and sugar vectors in G32. In most NMR structures of HIV-1 TAR (22–25,32,74,75), G32 adopts a looped out conformation. Cyclin T1 interacts with the U31 side of the apical loop (6), so the elevated mobility at G32 may be important for adaptive binding. The looped out G32 may also be involved in binding the nucleocapsid protein, which is known to interact with looped out guanine bases (76). Interestingly, a rather abrupt increase in stability is observed in the neighboring G33 residue (Fig. 4, *a* and *b*) particularly for its nucleobase, which in MD simulations also shows limited mobility and occasional stacking interactions.

Greater structural stability at the picosecond-nanosecond timescale is observed for C30 and G34, which exhibit low intensities and sizeable RDCs and S_{rel}^2 values (Fig. 4, *a* and *b*). However, the nucleobase of G34 also shows significant dispersion, consistent with a slower dynamical process occurring with a time constant of 30.9 ± 7.1 μs (Fig. 4 *c*). Biochemical studies (77) and MD simulations (53,78,79) suggest that C30 and G34 form a Watson-Crick basepair that is important for transcriptional activation (7). Although we were unable to observe the G34 imino proton, the fitting of the C30 and G34 RDCs to available NMR structures of TAR yields better agreement with structures in which the two bases are hydrogen bonded (data not shown). In MD simulations of TAR, the

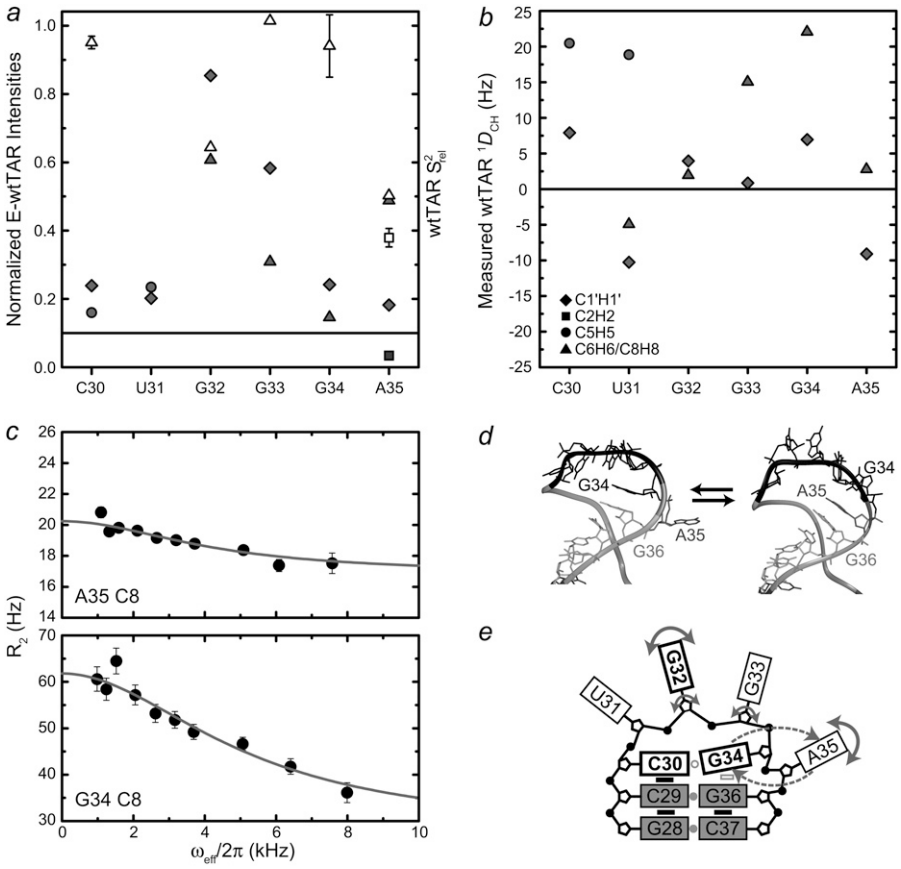

FIGURE 4 Dynamics of the wtTAR loop. Shown are the (*a*) normalized intensities for E-wtTAR (*solid symbols*) and S^2_{rel} values for nonelongated wtTAR (*open symbols*) and (*b*) one-bond C-H RDCs measured in the wtTAR loop (see *inset* for key). (*c*) Carbon R_2 as a function of field strength (ω_{eff}) for residues G34 (C8) and A35 (C8). Note that $R_2 = R_{2,int} + R_{ex} = R_{1\rho}/\sin^2\theta - R_1\tan^2\theta$. (*d*) Two snapshots from the 65 ns MD simulation of wtTAR illustrating the looping in and out of A35. (*e*) Schematic diagram of the observed wtTAR apical loop dynamics. Nucleobases, ribose moieties, and phosphate groups are represented by large rectangles, black pentagons, and solid black circles, respectively. Smaller black rectangles denote base-base stacking. Gray circles indicate hydrogen bonding between bases. The open gray rectangle indicates transient base-base stacking. The open gray circle indicates a transient hydrogen bond across the loop. Fast motions are indicated by solid arrows. The looping in and out of A35 and G34 is indicated by dashed arrows. Functionally important loop nucleotides are indicated by bolded labels and rectangles.

C30-G34 Watson-Crick basepair is observed to form transiently (39,53) and the observed G34 dispersion likely reflects the dynamics of basepair formation (Fig. 4 *c*).

Residue A35, which has been shown to be a critical spacer for transactivation (7) exhibits the most complex dynamics (Fig. 4, *a* and *b*). The near zero RDCs observed for both the C2 and C8 vectors suggest they undergo very large motional amplitudes (Fig. 4 *b*). Though the low S^2_{rel} values observed for these carbons are consistent with fast picosecond-nanosecond motions, these carbon nuclei also exhibit significant relaxation dispersion or reduced intensities in E-wtTAR, consistent with a slower dynamical process occurring with a time constant of 37.7 $\pm$ 10.2 μs (Fig. 4, *a* and *c*). The similarity of the timescales for A35 (37.7 μs) and G34 (30.9 μs) suggests that they may be undergoing a concerted dynamical process. In MD simulations, we observe concerted looping in and out motions in which G34 and A35 displace one another from a looped in conformation (Fig. 4 *d*). More limited motions are observed for U31, which in NMR structures and MD simulations of TAR is involved in stacking interactions with G32 for the majority of the time (Fig. 4 *d*).

CONCLUSION

Despite its small size, TAR exhibits a remarkable degree of structural and dynamical complexity that is important for the recognition of diverse targets. So far, the majority of biophysical studies have focused on characterizing dynamics at the UCU bulge and its importance in adaptive binding. However, few studies have quantitatively characterized the dynamics of the CUGGGA apical loop binding site and its potential role in adaptive recognition. The high flexibility at these two distinct binding sites may also give rise to motional correlations between them, as suggested previously (38,39). Such long-range motional correlations are increasingly implicated in the functions of RNA and are notoriously difficult to characterize experimentally.

Our study outlines a general NMR approach that can be used for studying long-range motional correlations. Here, strategic mutations are introduced at a given site and the consequent effects on structural dynamics at distant sites are quantified site-specifically using NMR measurements. Our results suggest that the TAR apical loop and bulge largely act as independent dynamical centers but do not entirely rule out the presence of transient long-range interactions between the apical loop and lower stem seen in MD simulations (39) and the NOE-based NMR structure of TAR (32), which may potentially indirectly affect the conformation of the intervening bulge linker. Such long-range interactions could provide a general mechanism for creating motional couplings between the apical loops and internal loop junctions.

The TAR apical loop is structurally heterogeneous and undergoes highly complex dynamics with different residues exhibiting very distinct dynamical behaviors over picosecond-millisecond timescales (Fig. 4 *e*). These motions render the apical loop highly malleable and ready for conformational adaptation that may allow recognition of diverse targets. Insights into the structural adaptability of the apical loop are beginning to emerge from structures of TAR complexes. For example, an NMR structure of HIV-2 TAR bound to a cyclic neooligoaminodeoxysaccharide shows that the loop undergoes a large conformational change, particularly at residues G32 and G33, which generally becomes ordered upon binding (36). Structures of TAR kissing complexes also show the apical loop residues involved in basepairing and assuming a geometry similar to that of an A-form helix (37,80). Future studies will likely show that in analogy to the highly flexible TAR bulge, the apical loop can adopt highly different conformations and thereby provide a molecular basis for binding a variety of protein targets. The flexibility of the TAR apical loop uncovered in this study should also provide useful guidelines for rationally designing TAR targeting anti-HIV therapeutics.

SUPPLEMENTARY MATERIAL

To view all of the supplemental files associated with this article, visit www.biophysj.org.

We thank members of the Al-Hashimi lab for insightful comments and help, and Dr. Alex Kurochkin for maintenance of the NMR instruments.

This work was supported by funding from the National Institutes of Health (NIH) (RO1 AI066975-01) to H.M.A. and the National Science Foundation (NSF) (CHE-0548047). The Michigan Economic Development Cooperation and the Michigan Technology Tri-Corridor supported and purchased the 600 MHz spectrometer. I.A. is grateful for the support of the NSF CAREER Award program, grant CHE-0548047. C.M. was supported by funding from the NIH-sponsored Molecular Biophysics Training Grant.

REFERENCES

1. Muesing, M. A., D. H. Smith, and D. J. Capon. 1987. Regulation of mRNA accumulation by a human immunodeficiency virus trans-activator protein. *Cell*. 48:691–701.
2. Bannwarth, S., and A. Gatignol. 2005. HIV-1 TAR RNA: the target of molecular interactions between the virus and its host. *Curr. HIV Res.* 3:61–71.
3. Karn, J. 1999. Tackling Tat. *J. Mol. Biol.* 293:235–254.
4. Jones, K. A. 1997. Taking a new TAK on Tat transactivation. *Genes Dev.* 11:2593–2599.
5. Majello, B., G. Napolitano, A. Giordano, and L. Lania. 1999. Transcriptional regulation by targeted recruitment of cyclin-dependent CDK9 kinase in vivo. *Oncogene*. 18:4598–4605.
6. Richter, S., Y. H. Ping, and T. M. Rana. 2002. TAR RNA loop: a scaffold for the assembly of a regulatory switch in HIV replication. *Proc. Natl. Acad. Sci. USA*. 99:7928–7933.
7. Richter, S., H. Cao, and T. M. Rana. 2002. Specific HIV-1 TAR RNA loop sequence and functional groups are required for human cyclin T1-Tat-TAR ternary complex formation. *Biochemistry*. 41:6391–6397.
8. Kim, I., C. W. Liu, and J. D. Puglisi. 2006. Specific recognition of HIV TAR RNA by the dsRNA binding domains (dsRBD1-dsRBD2) of PKR. *J. Mol. Biol.* 358:430–442.
9. Chang, Y. N., D. J. Kenan, J. D. Keene, A. Gatignol, and K. T. Jeang. 1994. Direct interactions between autoantigen La and human immunodeficiency virus leader RNA. *J. Virol.* 68:7008–7020.
10. Erard, M., D. G. Barker, F. Amalric, K. T. Jeang, and A. Gatignol. 1998. An Arg/Lys-rich core peptide mimics TRBP binding to the HIV-1 TAR RNA upper-stem/loop. *J. Mol. Biol.* 279:1085–1099.
11. Kanevsky, I., F. Chaminade, D. Ficheux, A. Moumen, R. Gorelick, M. Negroni, J. L. Darlix, and P. Fosse. 2005. Specific interactions between HIV-1 nucleocapsid protein and the TAR element. *J. Mol. Biol.* 348: 1059–1077.
12. Ben-Asouli, Y., Y. Banai, H. Hauser, and R. Kaempfer. 2000. Recognition of 5′-terminal TAR structure in human immunodeficiency virus-1 mRNA by eukaryotic translation initiation factor 2. *Nucleic Acids Res.* 28:1011–1018.
13. Andersen, E. S., S. A. Contera, B. Knudsen, C. K. Damgaard, F. Besenbacher, and J. Kjems. 2004. Role of the *trans*-activation response element in dimerization of HIV-1 RNA. *J. Biol. Chem.* 279:22243–22249.
14. Song, R., J. Kafaie, and M. Laughrea. 2008. Role of the 5′ TAR stem-loop and the U5-AUG duplex in dimerization of HIV-1 genomic RNA. *Biochemistry*. 47:3283–3293.
15. Puglisi, J. D., R. Tan, B. J. Calnan, A. D. Frankel, and J. R. Williamson. 1992. Conformation of the TAR RNA-arginine complex by NMR spectroscopy. *Science*. 257:76–80.
16. Williamson, J. R. 2000. Induced fit in RNA-protein recognition. *Nat. Struct. Biol.* 7:834–837.
17. Perez-Canadillas, J. M., and G. Varani. 2001. Recent advances in RNA-protein recognition. *Curr. Opin. Struct. Biol.* 11:53–58.
18. Long, K. S., and D. M. Crothers. 1999. Characterization of the solution conformations of unbound and Tat peptide-bound forms of HIV-1 TAR RNA. *Biochemistry*. 38:10059–10069.
19. Zacharias, M., and P. J. Hagerman. 1995. Bulge-induced bends in RNA: quantification by transient electric birefringence. *J. Mol. Biol.* 247:486–500.
20. Ippolito, J. A., and T. A. Steitz. 1998. A 1.3-angstrom resolution crystal structure of the HIV-1 *trans*-activation response region RNA stem reveals a metal ion-dependent bulge conformation. *Proc. Natl. Acad. Sci. USA*. 95:9819–9824.
21. Edwards, T. E., and S. T. Sigurdsson. 2003. EPR spectroscopic analysis of TAR RNA-metal ion interactions. *Biochem. Biophys. Res. Commun.* 303:721–725.
22. Faber, C., H. Sticht, K. Schweimer, and P. Rosch. 2000. Structural rearrangements of HIV-1 Tat-responsive RNA upon binding of neomycin B. *J. Biol. Chem.* 275:20660–20666.
23. Du, Z., K. E. Lind, and T. L. James. 2002. Structure of TAR RNA complexed with a Tat-TAR interaction nanomolar inhibitor that was identified by computational screening. *Chem. Biol.* 9:707–712.
24. Davis, B., M. Afshar, G. Varani, A. I. Murchie, J. Karn, G. Lentzen, M. Drysdale, J. Bower, A. J. Potter, I. D. Starkey, T. Swarbrick, and F. Aboul-ela. 2004. Rational design of inhibitors of HIV-1 TAR RNA through the stabilisation of electrostatic ''hot spots''. *J. Mol. Biol.* 336: 343–356.
25. Murchie, A. I., B. Davis, C. Isel, M. Afshar, M. J. Drysdale, J. Bower, A. J. Potter, I. D. Starkey, T. M. Swarbrick, S. Mirza, C. D. Prescott, P. Vaglio, F. Aboul-ela, and J. Karn. 2004. Structure-based drug design targeting an inactive RNA conformation: exploiting the flexibility of HIV-1 TAR RNA. *J. Mol. Biol.* 336:625–638.
26. Olsen, G. L., D. C. Echodu, Z. Shajani, M. F. Bardaro Jr., G. Varani, and G. P. Drobny. 2008. Solid-state deuterium NMR studies reveal μs-ns motions in the HIV-1 transactivation response RNA recognition site. *J. Am. Chem. Soc.* 130:2896–2897.
27. Edwards, T. E., and S. T, Sigurdsson. 2002. Electron paramagnetic resonance dynamic signatures of TAR RNA-small molecule complexes

provide insight into RNA structure and recognition. *Biochemistry.* 41:14843–14847.

28. Zhang, Q., A. C. Stelzer, C. K. Fisher, and H. M. Al-Hashimi. 2007. Visualizing spatially correlated dynamics that directs RNA conformational transitions. *Nature*. 450:1263–1267.
29. Zhang, Q., X. Sun, E. D. Watt, and H. M. Al-Hashimi. 2006. Resolving the motional modes that code for RNA adaptation. *Science*. 311: 653–656.
30. Al-Hashimi, H. M., Y. Gosser, A. Gorin, W. Hu, A. Majumdar, and D. J. Patel. 2002. Concerted motions in HIV-1 TAR RNA may allow access to bound state conformations: RNA dynamics from NMR residual dipolar couplings. *J. Mol. Biol.* 315:95–102.
31. Dayie, K. T., A. S. Brodsky, and J. R. Williamson. 2002. Base flexibility in HIV-2 TAR RNA mapped by solution ^{15}N, ^{13}C NMR relaxation. *J. Mol. Biol.* 317:263–278.
32. Aboul-ela, F., J. Karn, and G. Varani. 1996. Structure of HIV-1 TAR RNA in the absence of ligands reveals a novel conformation of the trinucleotide bulge. *Nucleic Acids Res.* 24:3974–3981.
33. Al-Hashimi, H. M., A. Gorin, A. Majumdar, Y. Gosser, and D. J. Patel. 2002. Towards structural genomics of RNA: rapid NMR resonance assignment and simultaneous RNA tertiary structure determination using residual dipolar couplings. *J. Mol. Biol.* 318:637–649.
34. Mei, H. Y., M. Cui, A. Heldsinger, S. M. Lemrow, J. A. Loo, K. A. Sannes-Lowery, L. Sharmeen, and A. W. Czarnik. 1998. Inhibitors of protein-RNA complexation that target the RNA: specific recognition of human immunodeficiency virus type 1 TAR RNA by small organic molecules. *Biochemistry.* 37:14204–14212.
35. Litovchick, A., A. G. Evdokimov, and A. Lapidot. 2000. Aminoglycoside-arginine conjugates that bind TAR RNA: synthesis, characterization, and antiviral activity. *Biochemistry.* 39:2838–2852.
36. Raghunathan, D., V. M. Sanchez-Pedregal, J. Junker, C. Schwiegk, M. Kalesse, A. Kirschning, and T. Carlomagno. 2006. TAR-RNA recognition by a novel cyclic aminoglycoside analogue. *Nucleic Acids Res.* 34:3599–3608.
37. Lebars, I., T. Richard, C. Di Primo, and J. J. Toulme. 2007. NMR structure of a kissing complex formed between the TAR RNA element of HIV-1 and a LNA-modified aptamer. *Nucleic Acids Res.* 35:6103–6114.
38. Huthoff, H., F. Girard, S. S. Wijmenga, and B. Berkhout. 2004. Evidence for a base triple in the free HIV-1 TAR RNA. *RNA*. 10:412–423.
39. Musselman, C., H. M. Al-Hashimi, and I. Andricioaei. 2007. iRED analysis of TAR RNA reveals motional coupling, long-range correlations, and a dynamical hinge. *Biophys. J.* 93:411–422.
40. Tinsley, R. A., and N. G. Walter. 2007. Long-range impact of peripheral joining elements on structure and function of the hepatitis delta virus ribozyme. *Biol. Chem.* 388:705–715.
41. Rueda, D., G. Bokinsky, M. M. Rhodes, M. J. Rust, X. Zhuang, and N. G. Walter. 2004. Single-molecule enzymology of RNA: essential functional groups impact catalysis from a distance. *Proc. Natl. Acad. Sci. USA*. 101:10066–10071.
42. Delaglio, F., S. Grzesiek, G. W. Vuister, G. Zhu, J. Pfeifer, and A. Bax. 1995. NMRpipe—a multidimensional spectral processing system based on UNIX pipes. *J. Biomol. NMR*. 6:277–293.
43. Goddard, T. D., and D. G. Kneller. 2004. SPARKY 3. University of California, San Francisco.
44. Furtig, B., C. Richter, J. Wohnert, and H. Schwalbe. 2003. NMR spectroscopy of RNA. *ChemBioChem.* 4:936–962.
45. Sklenar, V., R. D. Peterson, M. R. Rejante, and J. Feigon. 1993. Two- and three-dimensional HCN experiments for correlating base and sugar resonances in ^{15}N,^{13}C-labeled RNA oligonucleotides. *J. Biomol. NMR*. 3:721–727.
46. Wohnert, J., M. Gorlach, and H. Schwalbe. 2003. Triple resonance experiments for the simultaneous correlation of H6/H5 and exchangeable protons of pyrimidine nucleotides in ^{13}C,^{15}N-labeled RNA applicable to larger RNA molecules. *J. Biomol. NMR*. 26:79–83.
47. Meissner, A., and O. W. Sorensen. 1999. The role of coherence transfer efficiency in design of TROSY-type multidimensional NMR experiments. *J. Magn. Reson.* 139:439–442.
48. Pitt, S. W., Q. Zhang, D. J. Patel, and H. M. Al-Hashimi. 2005. Evidence that electrostatic interactions dictate the ligand-induced arrest of RNA global flexibility. *Angew. Chem. Int. Ed. Engl.* 44:3412–3415.
49. Hansen, M. R., P. Hanson, and A. Pardi. 2000. Filamentous bacteriophage for aligning RNA, DNA, and proteins for measurement of nuclear magnetic resonance dipolar coupling interactions. *Methods Enzymol.* 317:220–240.
50. Clore, G. M., M. R. Starich, and A. M. Gronenborn. 1998. Measurement of residual dipolar couplings of macromolecules aligned in the nematic phase of a colloidal suspension of rod-shaped viruses. *J. Am. Chem. Soc.* 120:10571–10572.
51. Getz, M., X. Sun, A. Casiano-Negroni, Q. Zhang, and H. M. Al-Hashimi. 2007. Review NMR studies of RNA dynamics and structural plasticity using NMR residual dipolar couplings. *Biopolymers.* 86:384–402.
52. Casiano-Negroni, A., X. Sun, and H. M. Al-Hashimi. 2007. Probing Na^+-induced changes in the HIV-1 TAR conformational dynamics using NMR residual dipolar couplings: new insights into the role of counterions and electrostatic interactions in adaptive recognition. *Biochemistry.* 46:6525–6535.
53. Musselman, C., S. W. Pitt, K. Gulati, L. L. Foster, I. Andricioaei, and H. M. Al-Hashimi. 2006. Impact of static and dynamic A-form heterogeneity on the determination of RNA global structural dynamics using NMR residual dipolar couplings. *J. Biomol. NMR*. 36:235–249.
54. Neidle, S. 1999. Oxford Handbook of Nucleic Acid Structure. Oxford University Press, New York.
55. Losonczi, J. A., M. Andrec, M. W. F. Fischer, and J. H. Prestegard. 1999. Order matrix analysis of residual dipolar couplings using singular value decomposition. *J. Magn. Reson.* 138:334–342.
56. Hansen, A. L., and H. M. Al-Hashimi. 2006. Insight into the CSA tensors of nucleobase carbons in RNA polynucleotides from solution measurements of residual CSA: towards new long-range orientational constraints. *J. Magn. Reson.* 179:299–307.
57. Bailor, M. H., C. Musselman, A. L. Hansen, K. Gulati, D. J. Patel, and H. M. Al-Hashimi. 2007. Characterizing the relative orientation and dynamics of RNA A-form helices using NMR residual dipolar couplings. *Nat. Protocols.* 2:1536–1546.
58. Palmer 3rd, A. G., and F. Massi. 2006. Characterization of the dynamics of biomacromolecules using rotating-frame spin relaxation NMR spectroscopy. *Chem. Rev.* 106:1700–1719.
59. Fushman, D., N. Tjandra, and D. Cowburn. 1999. An approach to direct determination of protein dynamics from N-15 NMR relaxation at multiple fields, independent of variable N-15 chemical shift anisotropy and chemical exchange contributions. *J. Am. Chem. Soc.* 121:8577–8582.
60. Hansen, A. L., and H. M. Al-Hashimi. 2007. Dynamics of large elongated RNA by NMR carbon relaxation. *J. Am. Chem. Soc.* 129:16072–16082.
61. MacKerell, A. D., N. Banavali, and N. Foloppe. 2000. Development and current status of the CHARMM force field for nucleic acids. *Biopolymers.* 56:257–265.
62. Jorgensen, W. L., J. Chandrasekhar, J. D. Madura, R. W. Impey, and M. L. Klein. 1983. Comparison of simple potential functions for simulating liquid water. *J. Chem. Phys.* 79:926–935.
63. Brooks, C. L., and M. Karplus. 1983. Deformable stochastic boundaries in molecular-dynamics. *J. Chem. Phys.* 79:6312–6325.
64. Nose, S. 1984. A unified formulation of the constant temperature molecular-dynamics methods. *J. Chem. Phys.* 81:511–519.
65. Hoover, W. G. 1985. Canonical dynamics—equilibrium phase-space distributions. *Phys. Rev. A*. 31:1695–1697.
66. Weeks, K. M., C. Ampe, S. C. Schultz, T. A. Steitz, and D. M. Crothers. 1990. Fragments of the HIV-1 Tat protein specifically bind TAR RNA. *Science*. 249:1281–1285.

67. Pitt, S. W., A. Majumdar, A. Serganov, D. J. Patel, and H. M. Al Hashimi. 2004. Argininamide binding arrests global motions in HIV-1 TAR RNA: comparison with Mg^{2+}-induced conformational stabilization. *J. Mol. Biol.* 338:7–16.

68. Tjandra, N., and A. Bax. 1997. Direct measurement of distances and angles in biomolecules by NMR in a dilute liquid crystalline medium. *Science.* 278:1111–1114.

69. Tolman, J. R., J. M. Flanagan, M. A. Kennedy, and J. H. Prestegard. 1995. Nuclear magnetic dipole interactions in field-oriented proteins—information for structure determination in solution. *Proc. Natl. Acad. Sci. USA.* 92:9279–9283.

70. Tolman, J. R., H. M. Al-Hashimi, L. E. Kay, and J. H. Prestegard. 2001. Structural and dynamic analysis of residual dipolar coupling data for proteins. *J. Am. Chem. Soc.* 123:1416–1424.

71. Lipari, G., and A. Szabo. 1982. Model-free approach to the interpretation of nuclear magnetic resonance relaxation in macromolecules. 1. Theory and range of validity. *J. Am. Chem. Soc.* 104:4546–4559.

72. Getz, M. M., A. J. Andrews, C. A. Fierke, and H. M. Al-Hashimi. 2006. Structural plasticity and Mg^{2+} binding properties of RNase P P4 from combined analysis of NMR residual dipolar couplings and motionally decoupled spin relaxation. *RNA.*13:251–266.

73. Reference deleted in proof.

74. Aboul-ela, F., J. Karn, and G. Varani. 1995. The structure of the human-immunodeficiency-virus type-1 TAR RNA reveals principles of RNA recognition by Tat protein. *J. Mol. Biol.* 253:313–332.

75. Brodsky, A. S., and J. R. Williamson. 1997. Solution structure of the HIV-2 TAR-argininamide complex. *J. Mol. Biol.* 267:624–639.

76. De Guzman, R. N., Z. R. Wu, C. C. Stalling, L. Pappalardo, P. N. Borer, and M. F. Summers. 1998. Structure of the HIV-1 nucleocapsid protein bound to the SL3 psi-RNA recognition element. *Science.* 279:384–388.

77. Kulinski, T., M. Olejniczak, H. Huthoff, L. Bielecki, K. Pachulska-Wieczorek, A. T. Das, B. Berkhout, and R. W. Adamiak. 2003. The apical loop of the HIV-1 TAR RNA hairpin is stabilized by a cross-loop base pair. *J. Biol. Chem.* 278:38892–38901.

78. Critchley, A. D., I. Haneef, D. J. Cousens, and P. G. Stockley. 1993. Modeling and solution structure probing of the HIV-1 TAR stem-loop. *J. Mol. Graph.* 11:92–97, 124.

79. Nifosi, R., C. M. Reyes, and P. A. Kollman. 2000. Molecular dynamics studies of the HIV-1 TAR and its complex with argininamide. *Nucleic Acids Res.* 28:4944–4955.

80. Chang, K. Y., and I. Tinoco Jr. 1997. The structure of an RNA ''kissing'' hairpin complex of the HIV TAR hairpin loop and its complement. *J. Mol. Biol.* 269:52–66.